AIP | Review of Scientific Instruments

Experimental measurements and noise analysis of a cryogenic radiometer

S. M. Carr, S. I. Woods, T. M. Jung, A. C. Carter, and R. U. Datla

Citation: Review of Scientific Instruments **85**, 075105 (2014); doi: 10.1063/1.4883191
View online: http://dx.doi.org/10.1063/1.4883191
View Table of Contents: http://scitation.aip.org/content/aip/journal/rsi/85/7?ver=pdfcov
Published by the AIP Publishing

Experimental measurements and noise analysis of a cryogenic radiometer

S. M. Carr,[a] S. I. Woods, T. M. Jung,[b] A. C. Carter,[b] and R. U. Datla[c]
National Institute of Standards and Technology (NIST), 100 Bureau Drive, Gaithersburg, Maryland 20899, USA

(Received 15 March 2014; accepted 27 May 2014; published online 10 July 2014)

A cryogenic radiometer device, intended for use as part of an electrical-substitution radiometer, was measured at low temperature. The device consists of a receiver cavity mechanically and thermally connected to a temperature-controlled stage through a thin-walled polyimide tube which serves as a weak thermal link. With the temperature difference between the receiver and the stage measured in millikelvin and the electrical power measured in picowatts, the measured responsivity was 4700 K/mW and the measured thermal time constant was 14 s at a stage temperature of 1.885 K. Noise analysis in terms of Noise Equivalent Power (NEP) was used to quantify the various fundamental and technical noise contributions, including phonon noise and Johnson-Nyquist noise. The noise analysis clarifies the path toward a cryogenic radiometer with a noise floor limited by fundamental phonon noise, where the magnitude of the phonon NEP is 6.5 fW/$\sqrt{\text{Hz}}$ for the measured experimental parameters. [http://dx.doi.org/10.1063/1.4883191]

I. INTRODUCTION

A thermal detector of optical radiation converts incident radiation into thermal energy through absorption, thereby raising the temperature of some element of the detector. The change in temperature is then converted to an electrical signal that can be amplified and displayed.[1] Here, the term optical radiation is generally defined as electromagnetic radiation obeying the laws of optics and covering the spectral range from the ultraviolet to the far-infrared.

A particular type of thermal detector is the bolometer, which consists of a radiation absorber and a thermometer, and which typically generates an electrical signal due to the temperature dependence of the electrical resistance of its active element. The original bolometer of Langley[2] evidently used a platinum ribbon as the resistive element. In that original work,[2] it was noted that "An instrument a thousand times more sensitive to radiant heat than the thermopile, and capable of indicating a change in temperature as minute as 1-100 000th of single Centigrade degree, deserves the attention of the physicist." The nature of the resistive material has evolved over time to include metals, semiconductors, and more recently superconductors.[3] Generally, the sensitivity of a bolometer may be improved through cryogenic operation.[4,5] Cryogenic bolometry and thermometry continue to be active areas of research and development.[6–14]

A radiometer may be distinguished from a bolometer, as a radiometer generally consists of an electrical heater in addition to a radiation absorber and a thermometer. Whereas a bolometer has no inherent capability of calibration, a radiometer is an instrument that may be used for measuring radiation in energy or power units. The addition of an electrical heater enables an inherent capability of calibration, because the detector can be heated electrically until the signal and thus the temperature rise equals that due to the unknown radiant power. Alternatively, the temperature of the detector may be controlled in a feedback loop, such that the rise in temperature due to the unknown radiant power is compensated by a reduced electrical power to the heater, in order to maintain the steady-state at the original temperature without incident radiation. For either mode of operation, the substituted electrical power is measured and the unknown magnitude of radiant power is equated to it. This method is therefore often referred to as electrical-substitution radiometry.

The technique of electrical-substitution radiometry, which can be traced back to early work by Angstrom[15] and Kurlbaum,[16] is used to measure the incident radiant power in absolute units. Kurlbaum[16] succinctly described the operation of his device as follows: "The temperature rise of the bolometer, which is caused by the incident radiation, can also be produced by means of an electric current. Consequently, radiation may be compared with an electric current. The quantities determining the current are measurable absolutely and one will therefore be able to express the radiation in absolute measure." Measurement in absolute units has motivated the use of the term *absolute radiometry* as an alternative to the term *electrical-substitution radiometry*. Absolute radiometry may be specifically defined as "the use of electrically calibrated thermal detectors of optical radiation for the realization of an optical power scale."[17] Absolute radiometry is one of the few techniques that can be used to measure the radiant power or radiant power per unit area in a beam of optical radiation in absolute units.

Absolute Cryogenic Radiometers (ACRs) have been developed and operated as primary standard reference detectors at the National Institute of Standards and Technology (NIST) over the last several decades.[18–26] The ACRs at NIST have been utilized for maintenance of the US standard for infrared radiant power in low-background environments, for measurement of the radiant power output of cryogenic blackbodies, for remote sensing detectors, and for general calibration and

[a]Present address: Sandia National Laboratories, Albuquerque, New Mexico 87123, USA.
[b]Present address: Jung Research and Development Corp., 1706 U St. NW #204, Washington, DC 20009, USA.
[c]Present address: NOAA/NESDIS/STAR, College Park, MD 20737, USA.

research activity in the infrared spectral region. An ACR may be partially characterized in terms of the responsivity and the thermal time constant. Responsivity is defined as the temperature change of the receiver for a given change in power and is in general a function of temperature. The thermal time constant is nominally the product of the thermal resistance and the heat capacity of the device, analogous to an electrical circuit where the time constant is the product of the electrical resistance and the capacitance. Measurements of an earlier NIST ACR, denoted here as ACRI,[18] revealed a responsivity of 30 K/mW and a thermal time constant of 27 s at a heat-sink temperature slightly above 2 K. Modeling and reengineering of ACRI led to a second-generation ACR, denoted as ACRII,[19] with measured responsivity of 210 K/mW and measured thermal time constant of 17 s at 2.2 K, achieving the desired goal of a more sensitive radiometer and thus the capability for lower-power measurement.

Motivated by the need for ultra-low-power cryogenic radiometers (CR) for metrological and radiometric purposes,[27–34] as well as the possibility of operating a cryogenic radiometer near fundamental noise limits,[1] we have designed, constructed, and measured a CR device that may serve as the basis for a next-generation ACR at NIST. The CR device consists of a receiver cavity with an electrical heater and resistive thermometer, a temperature-controlled heat sink with a calibrated resistive thermometer, and a weak thermal link between the receiver and the heat sink. The mechanical and thermal link between the receiver and the heat sink serves as thermal resistance that nominally determines the responsivity. Based on calculations[33] and initial measurements,[34] the material and structure chosen for the thermal link for this CR device is a thin-walled polyimide tube. Here, in this work, we show that the measured responsivity for the CR device is more than a factor of 20 larger than the measured responsivity for ACRII. An increase in the thermal responsivity would seemingly result in a corresponding increase in the thermal time constant. However, this CR device was designed such that reductions in the thermal mass and thus heat capacity would approximately offset the increased thermal resistance, such that the thermal time constant would remain manageable from a measurement perspective. This has been realized, as the measured thermal time constant at the lowest temperature is slightly less than the thermal time constant for ACRII. Using the measured experimental parameters for the CR device, we present a detailed noise analysis and quantitative evaluation of the various fundamental and technical Noise Equivalent Power (NEP) magnitudes, which clarifies the path toward an ultra-low-power cryogenic radiometer operated near fundamental noise limits.

In Sec. II, we describe the experimental configuration, including the physical components and the electrical circuits. Section III contains the experimental results of measurements at two temperatures, $T_0 = 4.311$ K and $T_0 = 1.885$ K, where T_0 is the temperature of the temperature-controlled stage measured using a calibrated temperature sensor. Measurements of the electrical heater resistance are used to define the numerical values of the resistance needed for computation of the power dissipated by the electrical heater. A thermal circuit model is used to aid in the extraction of responsivity and the thermal time constant. Section IV contains the noise analysis in terms of NEP. Since in this work there is no applied radiant input power, the NEP contributions are referred to the equivalent power fluctuation at the substitution heater. The relevant experimental, technical, and fundamental NEP magnitudes are analyzed and compared. Finally, in Sec. V we present our conclusions in the context of previous results and the ultimate objective of an ultra-low-power ACR operated near fundamental noise limits.

II. EXPERIMENTAL DESCRIPTION

The experimental platform shown in Fig. 1(a) was enclosed in the evacuated sample space of a liquid helium cryostat. At low temperature, the typical pressure in the sample space was less than or about 1.3×10^{-4} Pa. The bath temperature T_{bath} was reduced from about 4.2 K to about 1.8 K by pumping on the liquid helium. Partial thermal isolation between the Oxygen-Free-High-Thermal-Conductivity (OFHC) copper sample stage at temperature T_0 and the bath at temperature T_{bath} was enabled through the use of four aluminum legs connecting the sample stage to the cryostat. A resistor heater R_{stage} in combination with a germanium resistance thermometer R_{GRT} enabled control of the sample stage temperature T_0 using a standard Proportional-Integral-Derivative (PID) algorithm. The sample stage temperature was monitored by the Lake Shore Cryotronics[35] calibrated GRT[36] labeled $R_{cal\text{-}GRT}$.

A receiver cavity, intended for use as a component of a cryogenic radiometer, was mechanically and thermally connected to the sample stage through the thermal link shown in Fig. 1(a). An image of an actual device during the initial stages of assembly is shown in Fig. 1(b). The receiver cavity, in the shape of a hollow cone, has a base diameter of 4 mm and is made from electroformed copper plated with gold. The thermal link is a thin-walled polyimide tube[35,37] with inner diameter 1.02 mm, wall thickness 0.025 mm, and total length 8.4 mm. The inner diameter of the polyimide tube is approximately equal to both the outer diameter of the receiver cylinder and the outer diameter of the nipple on the sample stage, allowing the mating of these components with some overlap at both ends, as shown in Figs. 1(a) and 1(b). Subtracting the overlap lengths from the total length leaves approximately 6 mm without overlap. The mechanical and thermal joints between the receiver cylinder and the polyimide tube, as well as between the polyimide tube and the nipple on the sample stage, were made using GE[35] varnish.

Electrical power dissipated in the surface-mount heater resistor R_H, in combination with the finite thermal resistance of the device, enables the temperature difference $\Delta T \equiv (T - T_0)$ to be induced between the receiver cavity and the sample stage. This temperature difference was monitored by a bare-chip GRT resistance sensor R_G. Both R_H and R_G were mechanically and thermally attached to the receiver cone using GE[35] varnish. The electrical leads to R_H and R_G were 0.025 mm diameter copper-stabilized superconducting (SC) wire with a Nb-Ti superconducting core [$T_c = 9$ K] and copper sheath. The copper sheath was removed by etching except for short sections at the ends used for electrical contacts. Using SC lead wires allows four-terminal measurements

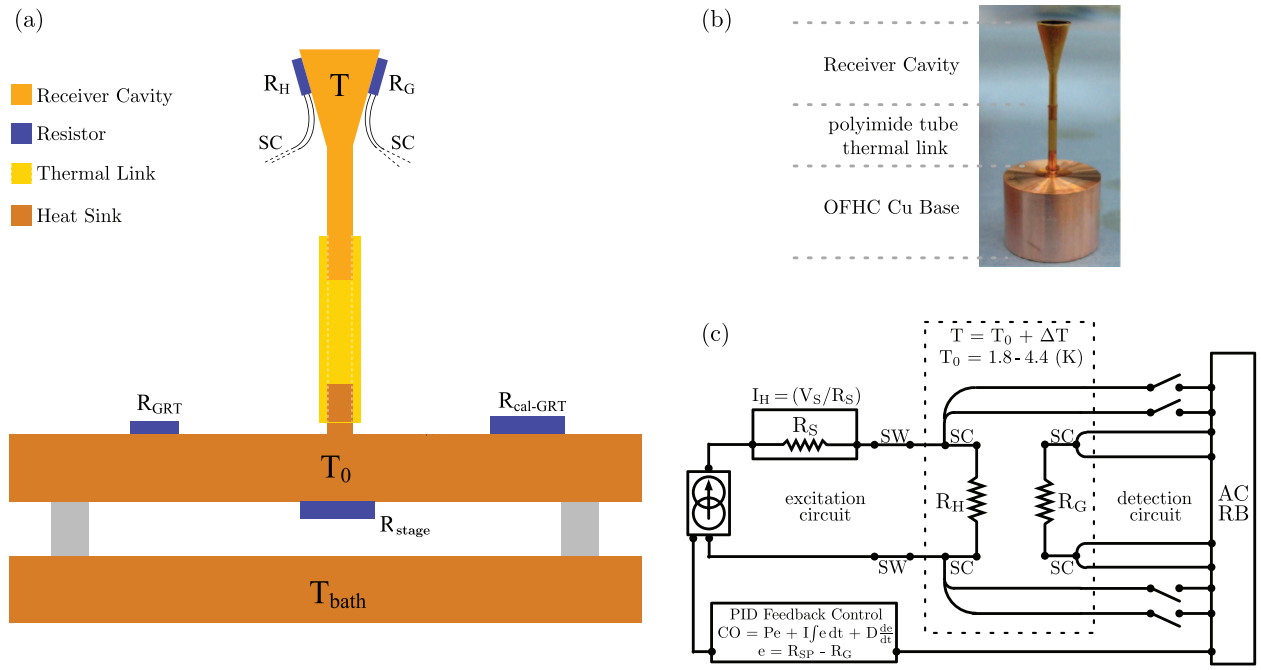

FIG. 1. Experimental apparatus used for the measurements. (a) Schematic showing the components of the experimental platform. Here, T refers to temperature, SC refers to superconducting, and the subscript GRT refers to germanium resistance thermometer. (b) Image of the device during the initial stages of assembly. Here, OFHC Cu refers to Oxygen-Free-High-Thermal-Conductivity copper. (c) Schematic of the electrical measurement circuits. Here, SW refers to switches, SC refers to superconducting, PID refers to Proportional-Integral-Derivative, and ACRB refers to AC resistance bridge. For other definitions refer to the text.

to be reduced to two-terminal measurements from the sample stage to the resistors R_H and R_G, which minimizes the number of electrical leads to the receiver cone, while enabling accurate resistance measurements and accurate measurement of the electrical power dissipated in the heater resistor. The SC lead wires were inserted through polyimide tubes with 0.127 mm inner diameter and 0.019 mm wall thickness for mechanical strain relief and electrical insulation.

A schematic of the electrical measurement circuits is shown in Fig. 1(c). We refer to the circuit with R_H as the excitation circuit and to the circuit with R_G as the detection circuit. A Lake Shore[35] Model 370 AC Resistance Bridge (ACRB) with the 3716L Low-Resistance Scanner was used for four-terminal resistance measurement of R_G within the detection circuit. After the stage temperature T_0 was stabilized, and with zero current in the excitation circuit, a measurement of R_G established the resistance value corresponding very nearly to thermal equilibrium $T = T_0$. The slight deviation from thermal equilibrium due to the finite power P_G dissipated in the measurement of R_G was minimized through exploration of the ACRB settings. This power was $P_G = 3.48$ pW for $T_0 = 4.311$ K and $P_G = 359$ fW for $T_0 = 1.885$ K. The temperature difference was computed from $\Delta T = \Delta R/(dR_G/dT)$ where ΔR is the difference between the measured R_G at temperature T and the measured R_G corresponding very nearly to temperature T_0. The sensitivity (dR_G/dT) was separately measured *in situ* at the two relevant temperatures, $T_0 = 4.311$ K and $T_0 = 1.885$ K, investigated in this work.

A low-noise DC current source, internal to the ACRB but a separate measurement circuit, was used as the heater output to drive DC current through the heater resistor R_H within the excitation circuit. The current I_H in the excitation circuit was measured using an Agilent[35] 3458A eight-digit multimeter operated as an ammeter in DC current mode. A current measurement with this ammeter is realized through the relation $I_H = (V_S/R_S)$ where V_S is the voltage across the internal shunt resistor R_S, as shown in Fig. 1(c). The heater resistance R_H in the excitation circuit was separately measured *in situ* using the ACRB after opening the switches (SW) in the excitation circuit and closing the four switches near the ACRB in Fig. 1(c), with the four terminals for the measurement of R_G disabled using internal relays. For measurements other than the measurement of R_H, the electrical circuits were operated as shown in Fig. 1(c).

From the measurements of the current I_H in the excitation circuit and the heater resistance R_H, the DC electrical power delivered to R_H is computed as $P_H = I_H^2 \cdot R_H$. This electrical power may be delivered in an open-loop or closed-loop configuration. Open-loop operation delivers constant electrical power without temperature feedback. Closed-loop operation utilizes electrical feedback to deliver the electrical power necessary to stabilize the temperature. The open-loop configuration has the advantage of simplified operation and possibly reduced noise, while the closed-loop configuration enables greater control but possibly at the expense of increased noise. For the results presented here, the excitation and detection circuits in Fig. 1(c) were operated in a closed-loop configuration using PID feedback control internal to the ACRB, with the controller output (CO) dependent on the error signal input $e = R_{SP} - R_G$, where R_{SP} is the resistance setpoint and R_G is the measured resistance of the GRT on the receiver.

III. EXPERIMENTAL RESULTS

We show in Fig. 2 the experimental measurements of the heater resistance R_H in the excitation circuit at the

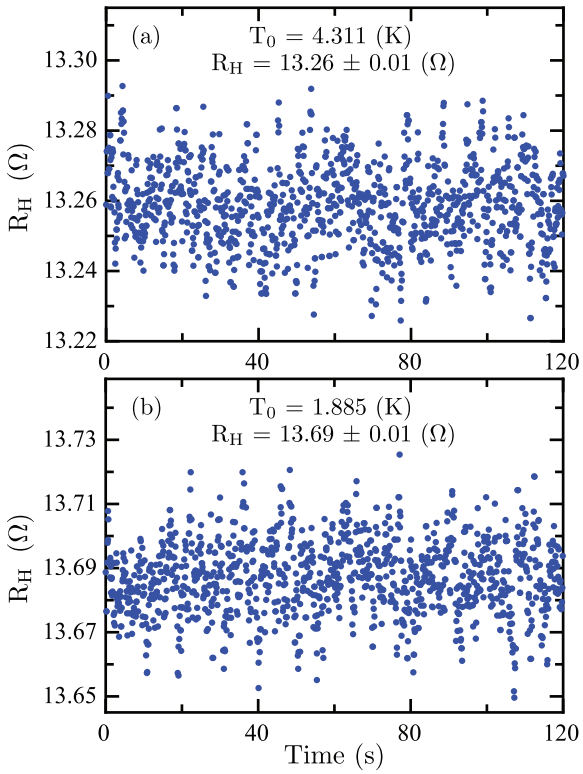

FIG. 2. Measured heater resistance R_H in the excitation circuit as a function of time at the temperatures (a) $T_0 = 4.311$ K and (b) $T_0 = 1.885$ K.

temperatures $T_0 = 4.311$ K and $T_0 = 1.885$ K. These data were acquired using four-terminal measurements with the ACRB, as described in Sec. II. The computed mean resistance value and standard deviation of the mean for the two temperatures are indicated in Figs. 2(a) and 2(b). Measurements of R_H before closed-loop operation were consistent with measurements of R_H after closed-loop operation.

Measurement of R_H at two distinct temperatures allows an estimate of the temperature sensitivity of the resistance $(dR_H/dT) \equiv \lim_{\Delta T \to 0}(\Delta R_H/\Delta T) \approx (\Delta R_H/\Delta T) = -0.177$ Ω/K. This estimate may be used to quantify the differences associated with deviations from thermal equilibrium, $T \neq T_0$, during the measurements. For the *in situ* measurements of R_H shown in Fig. 2, the power dissipated in the resistance measurement was approximately 1.3 pW. Using the measured thermal resistance values for the device (see below), this power may be converted into an equivalent temperature difference, $\Delta T \approx 0.005$ mK, which may in turn be converted to a difference in resistance through $[0.177\ \Omega/\text{K} \cdot 0.005\ \text{mK}] \approx 0.000001\ \Omega$, which is many orders-of-magnitude smaller than the resistance values indicated in Figs. 2(a) and 2(b). For the closed-loop results described below, the maximum temperature difference is on the order of 1 mK. This can be similarly converted to a difference in resistance through $[0.177\ \Omega/\text{K} \cdot 1\ \text{mK}] \approx 0.0002\ \Omega$, which is also many orders-of-magnitude smaller than the resistance values indicated in Figs. 2(a) and 2(b). These calculations indicate that any deviations in R_H from the measured values in Fig. 2 during closed-loop operation should be negligible compared to the measurement uncertainty of $\delta R_H = \pm 0.01\Omega$ indicated in Fig. 2. Therefore, the measured values of $R_H = 13.26\ \Omega$ at $T_0 = 4.311$ K and $R_H = 13.69\ \Omega$ at $T_0 = 1.885$ K are used in the subsequent analysis, in particular the computation of the electrical power $P_H = I_H^2 \cdot R_H$ delivered to R_H in closed-loop operation.

We show in Fig. 3 the measured steady-state and time-dependent thermophysical properties of the CR device, for two different stage temperatures, $T_0 = 4.311$ K and $T_0 = 1.885$ K. The plots in the left column show the results of steady-state measurements in closed-loop operation. These steady-state measurements allow extraction of the thermal resistance, or thermal responsivity, as described below. The minimum resolvable change in resistance ΔR, and therefore the minimum resolvable change in temperature through $\Delta T = \Delta R/(dR_G/dT)$, follows from the measured noise of $R_G(T_0)$ in thermal equilibrium. Starting from this minimum resolvable change in resistance, the resistance setpoint was incrementally increased resulting in an increased excitation current, and the excitation power delivered through the PID feedback control was recorded. As shown in the figures, the resulting power scale is picowatts with the temperature difference measured in millikelvin. The standard uncertainty in the measurement of ΔT was computed from the definition $\Delta T = \Delta R/(dR_G/dT)$ using the law of propagation of uncertainty,[38] resulting in the average standard uncertainties displayed as error bars in the legends of Figs. 3(a) and 3(c). The standard uncertainty in the electrical power, $P_H = I_H^2 \cdot R_H$, was computed using the same method. For Fig. 3(a), the relative statistical uncertainty in the electrical power ranges from 0.2% at the lowest power to 0.1% at the highest power. For Fig. 3(c), the relative statistical uncertainty in the electrical power ranges from 0.6% at the lowest power to 0.2% at the highest power. Thus, the error bars for the electrical power are negligibly small on the scale of the plots and are therefore not displayed.

After the steady-state measurements were completed for the highest electrical powers in Figs. 3(a) and 3(c), the control loop was turned off and the resulting return toward thermal equilibrium was recorded by monitoring the temperature difference as a function of time, as shown in Figs. 3(b) and 3(d). These time-dependent measurements allow extraction of the thermal response time, as described below. The standard uncertainty in the normalized temperature difference, $[\Delta T(t)/\Delta T(t = 0)]$, was also computed through the law of propagation of uncertainty. The average standard uncertainty in this quantity is shown as an error bar in the legends of Figs. 3(b) and 3(d).

A thermal detector of radiation, such as the CR device investigated in this work, operates by monitoring the temperature change induced in an active element by the absorption of radiation. A thermal circuit model, in analogy with an electrical circuit model, may be constructed by assuming that the device has heat capacity C and is connected to a heat sink at constant temperature T_0 through a thermal conductance G. If the power input to the detector is the time-dependent quantity $P(t)$, the time evolution of the temperature difference $\theta(t) \equiv \Delta T(t) \equiv [T(t) - T_0]$ is governed by[1]

$$C \frac{d\theta(t)}{dt} + G\,\theta(t) = P(t), \tag{1}$$

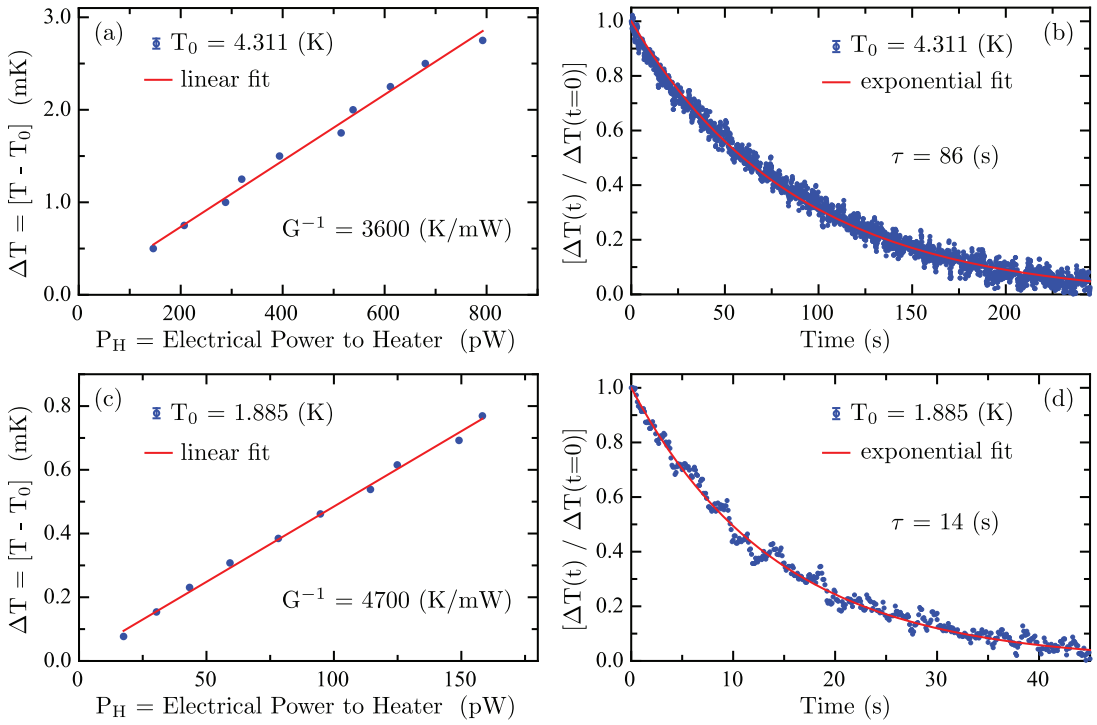

FIG. 3. Measured steady-state and time-dependent temperature difference as a function of the electrical power to the heater and as a function of time after the electrical power to the heater was shut off. The top row (a) and (b) is for $T_0 = 4.311$ K and the bottom row (c) and (d) is for $T_0 = 1.885$ K. The thermal responsivity G^{-1} is defined as the slope from the linear fits to the steady-state data and τ is the thermal time constant from the exponential fits to the time-dependent data.

where in general $P(t) = P_E(t) + P_R(t)$, with $P_E(t)$ the electrical power input and $P_R(t)$ the radiative power input. Here, there is no applied radiative input power, thus nominally $P_R(t) = 0$ and only the electrical power input need be considered. The electrical power input $P_E = P_H + P_G$ is dominated by the electrical power P_H delivered to the heater resistor R_H, where P_G is the electrical power dissipated in the resistance measurement of R_G. In the steady-state, Eq. (1) simplifies to

$$\theta \equiv [T - T_0] \equiv \Delta T = G^{-1} \cdot P_H + \theta_c. \quad (2)$$

Thus, a plot of ΔT versus P_H is predicted to be linear with slope G^{-1} and intercept θ_c. We fit the steady-state data in Figs. 3(a) and 3(c) according to Eq. (2) using a linear regression algorithm that accounts for the uncertainty in ΔT and the uncertainty in P_H. For $T_0 = 4.311$ K, the correlation coefficient is 0.9954 with slope $G^{-1} = 3600 \pm 200$ K/mW and intercept $\theta_c = 0.02 \pm 0.07$ mK. For $T_0 = 1.885$ K, the correlation coefficient is 0.9981 with slope $G^{-1} = 4700 \pm 200$ K/mW and intercept $\theta_c = 0.01 \pm 0.02$ mK. The uncertainties in the slope and intercept are the estimated standard deviations from the linear regression analysis that accounts for the underlying uncertainties in ΔT and P_H. The extracted values of G^{-1} may be referred to as the thermal resistance or thermal responsivity of the device.

As noted above, the time evolution for the return toward thermal equilibrium, where the initial value of the temperature difference corresponds to the maximum electrical power to the heater in the steady-state, is shown in Fig. 3(b) for $T_0 = 4.311$ K and in Fig. 3(d) for $T_0 = 1.885$ K. We solve Eq. (1) with $P_H = 0$, since the feedback control loop was turned off for these measurements, resulting in the time-dependent solution

$$\theta(t) \equiv [T(t) - T_0] \equiv \Delta T(t) = \Delta T(t{=}0) \cdot e^{-(t/\alpha\tau)} + \theta_c \cdot [1 - e^{-(t/\alpha\tau)}]. \quad (3)$$

In Eq. (3), the thermal response time τ is defined in the usual way through $\Delta T(\tau) \equiv e^{-1} \cdot \Delta T(t = 0)$, with the numerical factor $\alpha \equiv \{-\ln[(e^{-1}\Delta T(t = 0) - \theta_c)/(\Delta T(t = 0) - \theta_c)]\}^{-1}$. We fit the time-dependent data in Figs. 3(b) and 3(d) according to Eq. (3) using a Levenberg-Marquardt algorithm that accounts for the uncertainty in the normalized temperature difference $[\Delta T(t)/\Delta T(t = 0)]$, resulting in the values for τ indicated on the plots. Uncertainty analysis for Fig. 3(b) yields $\tau = 86 \pm 10$ s and $\theta_c = -0.03 \pm 0.08$ mK. Uncertainty analysis for Fig. 3(d) yields $\tau = 14 \pm 2$ s and $\theta_c = -0.002 \pm 0.02$ mK. Considering the $T_0 = 1.885$ K experimental data in Figs. 3(c) and 3(d), the combination of the relatively large thermal resistance of $G^{-1} = 4700$ K/mW and the relatively short thermal time constant of $\tau = 14$ s may be unprecedented for a cryogenic radiometer device of the type considered in this work.

IV. NOISE ANALYSIS

A. General characterization through NEP

An absolute cryogenic radiometer based on the device considered here enables measurement of radiative power with absolute accuracy through measurement of the electrical substitution power. The electrical substitution power is the difference between the DC electrical power without incident

radiation and the DC electrical power with incident radiation. It is therefore desirable to understand and quantify the noise present in the measurement of the electrical substitution power, as well as the other system noise sources, with all of the system noise contributions expressed as equivalent electrical-substitution noise powers. The individual noise contributions are characterized through the NEP,

$$\mathrm{NEP}^2 \equiv \frac{S_\mathrm{u}(f)}{\mathscr{R}_\mathrm{u}^2}, \tag{4}$$

where u is a generic variable with noise spectral density $S_\mathrm{u}(f)$ and responsivity $\mathscr{R}_\mathrm{u} \equiv (\delta \mathrm{u}/\delta \mathrm{P_H})$. For a radiometer in actual operation, all of the NEP contributions would naturally be referred to the radiative input power. In this work, there is no radiative input power, thus the NEP contributions considered here are referred to the equivalent power fluctuation at the substitution heater. In the following discussion of radiometer noise, the heat sink temperature will be taken as $\mathrm{T_0} = 1.885$ K, since this is the lowest measured temperature in this work and is at or near the temperature setpoint for a radiometer of this type used as a thermal-detector-based standard for infrared radiant power.

B. Experimental NEP

The experimentally measured values for the NEP may be computed by consideration of the measured quantities for the excitation (heater) and detection circuits and the relationship of these quantities to the heater power, $\mathrm{P_H}$, which is the power dissipated in the heater resistor $\mathrm{R_H}$; refer to Fig. 1. For the excitation circuit, the power dissipated in the heater resistor is computed as $\mathrm{P_H} = \mathrm{I_H^2\,R_H}$, where $\mathrm{R_H}$ is measured separately using the ACRB and is assumed constant during closed-loop operation. Thus, the measured quantity of interest in this case is $\mathrm{I_H}$, the current in the excitation circuit, with noise spectral density $S_\mathrm{I} = \sigma_\mathrm{I}^2/\mathrm{B_H}$, where $\sigma_\mathrm{I} \equiv (\delta \mathrm{I_H})_\mathrm{rms}$ is the measured standard deviation and $\mathrm{B_H}$ is the equivalent noise bandwidth[39] for the current measurement. Applying Eq. (4) to this case, the current responsivity is $\mathscr{R}_\mathrm{I} \equiv (\delta \mathrm{I_H}/\delta \mathrm{P_H}) = (2\,\mathrm{I_H\,R_H})^{-1}$, resulting in the expression

$$\mathrm{NEP}^2_{\mathrm{exp-H}} \equiv \frac{S_\mathrm{I}}{\mathscr{R}_\mathrm{I}^2} = (2\,\mathrm{I_H\,R_H})^2\,S_\mathrm{I} = 4\,S_\mathrm{I}\,\mathrm{R_H\,P_H} \tag{5}$$

for the experimental NEP for the excitation circuit. In Fig. 4, this experimental NEP is plotted versus the heater power, $\mathrm{P_H}$. For the detection circuit, the steady-state relation displayed in Eq. (2), $\Delta \mathrm{T} = \mathrm{G}^{-1} \cdot \mathrm{P_H} + \theta_c$, may be utilized to compute the experimental NEP. The measured quantity within the detection circuit is the resistance, $\mathrm{R_G}$, of the germanium resistance thermometer (GRT), with noise spectral density $S_\mathrm{R} = \sigma_\mathrm{R}^2/\mathrm{B_G}$, where $\sigma_\mathrm{R} \equiv (\delta \mathrm{R_G})_\mathrm{rms}$ is the measured standard deviation and $\mathrm{B_G}$ is the equivalent noise bandwidth[40] for the resistance measurement. The responsivity is $\mathscr{R}_\mathrm{R} \equiv (\delta \mathrm{R_G}/\delta \mathrm{P_H}) = \mathrm{G}^{-1}\,(\mathrm{dR_G/dT})$, where G is the thermal conductance. Applying Eq. (4) to this case results in the expression

$$\mathrm{NEP}^2_{\mathrm{exp-G}} \equiv \frac{S_\mathrm{R}}{\mathscr{R}_\mathrm{R}^2} = \left(\mathrm{G}\left(\frac{\mathrm{dR_G}}{\mathrm{dT}}\right)^{-1}\right)^2 S_\mathrm{R} = \mathrm{G}^2\left(\frac{\mathrm{dR_G}}{\mathrm{dT}}\right)^{-2} S_\mathrm{R} \tag{6}$$

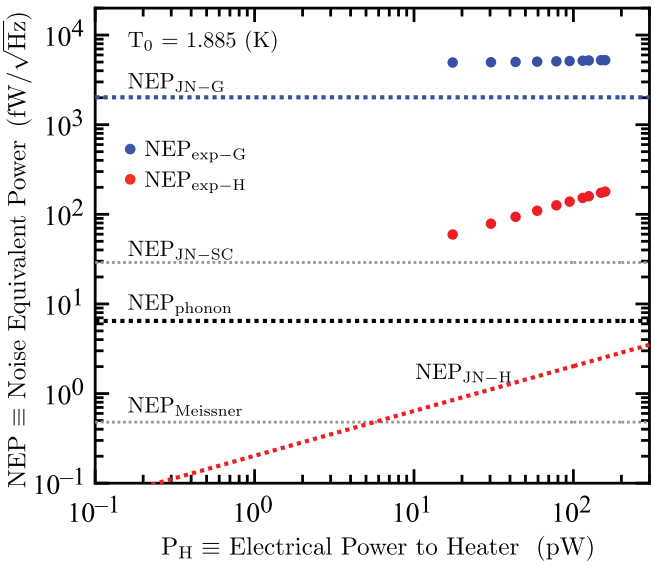

FIG. 4. Noise Equivalent Power (NEP) at $\mathrm{T_0} = 1.885$ K for the cryogenic radiometer device. The data points are the experimental (exp) NEP values computed from measured quantities. Here, the subscript G refers to the detection circuit, the subscript H refers to the excitation circuit, JN refers to Johnson-Nyquist noise, and SC refers to superconducting. The fundamental noise floor is due to phonon noise, denoted as $\mathrm{NEP_{phonon}}$, which is also referred to as temperature noise or thermal noise.

for the experimental NEP for the detection circuit. This experimental NEP, which is independent of the excitation power, is plotted in Fig. 4.

C. Fundamental and technical noise sources

There are various sources of fundamental and technical noise in a cryogenic electrical-substitution radiometer in operation as a thermal detector of radiation. In the absence of applied radiation, the only fundamental noise present in an ideal[1] thermal detector is temperature noise, also referred to as thermal noise or phonon noise. This noise is due to fluctuations in the temperature of the active element that occur even in thermal equilibrium, as required by the fluctuation-dissipation theorem or generalized Nyquist relation.[41,42] The thermal equilibrium spectral density of temperature noise is given by $S_\mathrm{T}(f) = 4\,k\,\mathrm{T}^2\,\mathrm{G}^{-1}$. As noted above, in this work there is no radiative input power, thus the NEP is referred to the equivalent electrical power fluctuation at the substitution heater. The thermal responsivity is therefore simply the thermal resistance: $\mathscr{R}_\mathrm{T} \equiv (\delta \mathrm{T}/\delta \mathrm{P_H}) = \mathrm{G}^{-1}$. An expression for nonequilibrium phonon noise, which accounts for the nonzero temperature gradient across the thermal link, has been derived by Mather,[43] with the result that the thermal-equilibrium squared-NEP is multiplied by a dimensionless prefactor, denoted here as γ, involving integrals containing the temperature and the thermal conductivity of the thermal link. Evaluating the integrals[43] analytically, we find $(1 - \gamma) \approx [2 \cdot (\Delta \mathrm{T}/\mathrm{T_0})] \lesssim 10^{-3}$ for the $\mathrm{T_0} = 1.885$ K data in Fig. 3(c), thus we use $\gamma = 1$. A value of γ close to unity may be intuitively understood from the fact that the experimental temperature difference across the thermal link is intentionally minimized in order to operate in the $(\Delta \mathrm{T}/\mathrm{T_0}) \ll 1$ regime. Applying Eq. (4),

TABLE I. Johnson-Nyquist (JN) noise expressions for the resistances in the heater (H) and detection (G) circuits.

R (Ω)	S_{JN} (V^2/Hz)	$\mathscr{R}_V$ (V/W)	$NEP^2_{JN} = S_{JN}/\mathscr{R}^2_V$ (W^2/Hz)
R_H	$4kTR_H$	$\frac{1}{2}(R_H/P_H)^{1/2}$	$16kTP_H$
R_S	$4kT_SR_S$	$\frac{1}{2}(R_S^2/R_HP_H)^{1/2}$	$16kT_S(R_H/R_S)P_H$
R_{HL}	$4kT_{HL}R_{HL}$	$\frac{1}{2}(R_{HL}^2/R_HP_H)^{1/2}$	$16kT_{HL}(R_H/R_{HL})P_H$
R_G	$4kTR_G$	$G^{-1}\left(\frac{P_G}{R_G}\right)^{1/2}\left(\frac{dR_G}{dT}\right)$	$4kT\left(\frac{G^2}{P_G}\right)\left(\frac{1}{R_G}\frac{dR_G}{dT}\right)^{-2}$
R_{GL}	$4kT_{GL}R_{GL}$	$G^{-1}\left(\frac{P_G}{R_G}\right)^{1/2}\left(\frac{dR_G}{dT}\right)$	$4kT_{GL}\left(\frac{G^2R_{GL}R_G}{P_G}\right)\left(\frac{dR_G}{dT}\right)^{-2}$

we therefore arrive at the following expression for the phonon NEP:

$$NEP^2_{phonon} = 4\,\gamma\,k\,T^2\,G \equiv 4\,\gamma\,k\,(T_0 + \Delta T)^2\,G \approx 4\,\gamma\,k\,T_0^2\,G. \tag{7}$$

The approximation in Eq. (7) follows from the fact that $(\Delta T/T_0) \ll 1$, as discussed above. For $\gamma = 1$, $T_0 = 1.885$ K, and the experimental value of $G^{-1} = 4700$ K/mW from Fig. 3(c), the magnitude of the phonon NEP is 6.5 fW/$\sqrt{\text{Hz}}$, as shown in Fig. 4.

An electrical-substitution radiometer effectively transfers an electrical power scale to a radiative power scale. The various resistances in the electrical circuits are sources of Johnson-Nyquist (JN) noise. Johnson found experimentally[44] that the thermal agitation of electrons in a resistor produce a fluctuating voltage across the resistor. Nyquist[45] derived an expression for this noise by considering the noise to be a one-dimensional form of blackbody radiation. The thermal-equilibrium formula derived by Nyquist is $S_{JN}(f) = 4\,k\,T\,R$, where T is the absolute temperature, R is the resistance, and $S_{JN}(f)$ is the spectral density of JN noise.

Referring to Fig. 1, and in particular to the electrical circuit schematic Fig. 1(c), JN noise will be associated with the explicit resistances R_H, R_S, and R_G. The lead resistance in the excitation circuit, R_{HL}, and the lead resistance in the detection circuit, R_{GL}, will also have associated JN noise. In Table I, we present formulas for JN noise associated with the individual resistances in the excitation and detection circuits, leading to expressions for the NEP. The voltage responsivity, $\mathscr{R}_V \equiv (\delta V/\delta P_H)$, is defined such that the NEP is referred to the equivalent power fluctuation at the substitution heater. Applying Eq. (4), the squared NEP for JN noise may be expressed as $NEP^2_{JN} = [S_{JN}/\mathscr{R}^2_V]$. From Fig. 2(b), the measured heater resistance is $R_H = 13.69$ Ω at the temperature $T \approx T_0 = 1.885$ K. The ammeter shunt resistance is $R_S = 5.2$ kΩ at room temperature $T_S = 294$ K. The approximate lead resistances are $R_{HL} = 15$ Ω and $R_{GL} = 10$ Ω. The effective temperatures, T_{HL} and T_{GL}, of the lead resistances are defined by evaluating the average spectral density of JN noise as an integral over the lead length, from the instruments at room temperature to the device at low temperature, resulting in the values $T_{HL} = 200\ K = T_{GL}$. For the purpose of calculating the JN noise properties, the average value of $R_G = 35\,260$ Ω is used for the resistance of the GRT, which required $P_G = 359$ fW of power dissipated for the resistance measurement. The sensitivity $(dR_G/dT) \equiv \lim_{\Delta T \to 0}(\Delta R_G/\Delta T) = -65\,000$ Ω/K was separately measured *in situ* using the PID temperature control of the sample stage and the calibrated GRT.

The JN NEP for the excitation and detection circuits may be calculated separately by adding in quadrature the various contributions in Table I. For the excitation circuit, the sum of the three contributions in Table I is dominated by the JN noise associated with the lead resistance in the excitation circuit, which may be verified by evaluating the two ratios of the three terms in Table I. The contribution associated with the lead resistance dominates the contribution associated with the heater resistance because of the temperature ratio, whereas it dominates the contribution associated with the shunt resistance because of the resistance ratio. The total NEP_{JN-H} for the excitation circuit, which is proportional to the square root of the heater power, is plotted in Fig. 4. For the detection circuit, there are two contributions, a contribution associated with the GRT resistance and a contribution associated with the lead resistance, as indicated in Table I. The ratio of these two terms is the product of a temperature ratio and a resistance ratio, with the net result that the GRT contribution dominates the lead resistance contribution. The total NEP_{JN-G} for the detection circuit, which is independent of the heater power, is plotted in Fig. 4.

D. Discussion of noise analysis results

There are several aspects of Fig. 4 that merit elaboration. Recall from the discussion above that, in the absence of applied radiation, the fundamental noise floor of a thermal detector is determined by the magnitude of phonon noise, as expressed in Eq. (7) and shown in Fig. 4 for the parameters studied in this work. From the perspective of radiometer design and engineering, the ultimate objective is to realize a thermal detector with technical noise magnitudes less than the fundamental phonon noise floor, thereby approaching the limit of the ideal[1] thermal detector.

In Fig. 4, the calculated NEP_{JN-H} for the excitation circuit is less than the phonon noise floor over the relevant range of heater power. This is positive in the sense that improvements in the excitation circuit electrical design and engineering would not necessarily need to address JN noise, since the calculated JN noise is already below the phonon noise floor. However, the experimental NEP_{exp-H} data points for the excitation circuit are approximately a factor of 70 larger than the calculated JN NEP and approximately a factor of 10-30 larger than the phonon noise floor over the measured range of heater power. Referring to Fig. 1(c), there are several possible instrumental or technical sources of noise, separate from the JN noise already considered, in the excitation circuit. Possible sources of noise include: (i) the DC current source, (ii) the DC ammeter, (iii) the specific cabling/wiring configuration, and (iv) closed-loop feedback noise. The measured current noise is about a factor of 10 greater than the maximum noise current specified by the manufacturer for the DC current source and about a factor of 1000 greater than the maximum noise current specified by the manufacturer for the DC ammeter. The extraneous noise is probably closed-loop feedback noise. In closed-loop operation, the PID controller requires

input in the form of a resistance or temperature setpoint and controls the current source output using the adjustable PID parameters. For this work, the derivative (D) term is set to zero to minimize noise. However, noise can be introduced in the feedback process[46] with finite proportional (P) and integral (I) terms, even with the derivative term set to zero. Adjustment of the proportional (P) and integral (I) terms, improved feedback electronics, and an improved detection circuit (see below), may enable excitation circuit NEP magnitudes near or below the phonon noise floor.

In contrast to the excitation circuit, it is apparent from Fig. 4 that the detection circuit is nearly JN-noise-limited. Specifically, the experimental NEP_{exp-G} magnitudes for the detection circuit are less than a factor of 3 larger than the calculated NEP_{JN-G} for the detection circuit over the measured range of heater power. The difference between the experimental NEP magnitudes and the calculated JN NEP is almost entirely accounted for by consideration of the ACRB instrumental noise. Applying Eq. (4) to the ACRB gives $NEP_{ACRB} = (S_V/\mathscr{R}_V^2)^{1/2} = [S_V G^2 P_G^{-1} R_G (dR_G/dT)^{-2}]^{1/2} = 4.2\,pW/\sqrt{Hz}$, where $\sqrt{S_V} = 4\ nV/\sqrt{Hz}$ is the input noise figure for the ACRB specified by the manufacturer. Adding NEP_{ACRB} in quadrature with NEP_{JN-G} for the detection circuit results in a value very close to the experimental NEP_{exp-G} for the detection circuit.

It is clear from Fig. 4 that the calculated NEP_{JN-G} for the detection circuit is more than two orders-of-magnitude larger than the fundamental phonon noise floor. Recall from the discussion above that the NEP_{JN-G} for the detection circuit shown in Fig. 4 is determined mainly by the JN noise associated with the GRT resistance, as expressed explicitly in Table I. That expression implies that the JN NEP is inversely proportional to the product $[(1/R_G)\cdot(dR_G/dT)]$. Using the measured values stated above, $R_G = 35\,260\ \Omega$ and $|(dR_G/dT)| = 65\,000\ \Omega/K$, results in the product $[(1/R_G)\cdot(dR_G/dT)] = 1.84\ K^{-1}$. Thus, although the derivative (slope) of the GRT R(T) curve is relatively large, the value of R(T) is also relatively large, resulting in rather modest values for the product and the corresponding JN NEP shown in Fig. 4. The measured value for the product is at or near the upper limit for a GRT, thus utilizing a different GRT or other conventional resistive thermometer is unlikely to result in significant reduction of the JN NEP toward the fundamental phonon noise floor.

Given the limitations of GRTs or other conventional resistive thermometers, we consider the potential of alternative thermometers in the context of Table I and Fig. 4. From Table I, the JN NEP for a resistive detection circuit may be written generally as $NEP_{JN}^2 = [(4kTR + 4kT_L R_L)\ (G^2/P)\ R\ (dR/dT)^{-2}]$. There are two limits of this expression, dependent on the value of the ratio $[(T/T_L)\ (R/R_L)]$ compared to unity. For $[(T/T_L)\ (R/R_L)] \ll 1$, the JN noise is limited by the NEP due to the lead resistance R_L at effective temperature T_L. For $[(T/T_L)\ (R/R_L)] \gg 1$, the JN NEP is inversely proportional to the product $[(1/R)\cdot(dR/dT)]$ as stated above, limited by the JN noise of the thermometer resistance at low temperature; this limit is realized in this work because of the large value of the GRT resistance compared to the lead resistance. It is also possible to realize this limit not by employing a relatively large thermometer resistance, but through minimization of the JN NEP due to lead resistance, for example, by utilizing inductive SQUID readout[47,48] at low temperature. Therefore, assuming the potential alternative detection circuit is operated in this limit, the JN NEP will be inversely proportional to the product $[(1/R)\cdot(dR/dT)]$. Thus, the JN NEP is minimized for the combination of a relatively small resistance and a relatively large sensitivity, which may be realized by utilizing a transition-edge-sensor (TES) based on the resistive SC transition.

For a resistive SC-TES, the product $[(1/R_{sc})\cdot(dR_{sc}/dT)]^{-1} = \alpha\cdot\delta T$, where α is a numerical factor and δT is the (90%–10%) temperature transition width. Substitution into the general NEP_{JN} above in the limit of $[(T/T_L)\ (R/R_L)] \gg 1$ results in $NEP_{JN-SC} = 2\alpha\cdot(kT/P_{sc})^{1/2}\cdot G\cdot\delta T$. In order to calculate a value for NEP_{JN-SC}, we assume that the ratio $(NEP_{JN-SC}/P_{sc}) = (NEP_{JN-G}/P_G) \approx 5$, the ratio found experimentally in this work. We also assume $\alpha = (1/3)$ and we use the experimental values, $T = 1.885$ K and $G^{-1} = 4700$ K/mW, from this work. The remaining parameter is δT, the transition width. Assuming $\delta T = 3$ mK results in $NEP_{JN-SC} = 29\ fW/\sqrt{Hz}$, which is approximately a factor of 70 smaller than NEP_{JN-G} and a factor of 4 larger than NEP_{phonon} in Fig. 4. A lower limit to the transition width[49,50] is perhaps $\delta T = 1$ mK, resulting in $NEP_{JN-SC} = 14\ fW/\sqrt{Hz}$, which is approximately a factor of 140 smaller than NEP_{JN-G} and a factor of 2 larger than NEP_{phonon} in Fig. 4. Therefore, a resistive SC-TES[51] appears to result in significantly reduced JN noise compared with the detection circuit JN noise floor shown in Fig. 4. However, reduction of the resistive SC-TES JN noise to or below the phonon noise floor in Fig. 4 appears to be challenging.

A promising potential alternative thermometer, which we have developed in our laboratory at NIST, is a SC-TES based on the magnetic superconducting transition. We refer to the device as the Meissner-TES,[8] because the temperature change of a superconducting element is monitored by measuring magnetic flux expulsion associated with the Meissner effect. The Meissner-TES operates by using a superconducting element with a sharp transition and by sensing the transition with a DC SQUID. By measuring the magnetic rather than the resistive transition of the superconducting element, it is possible for the element to be monitored in a noncontact manner, resulting in improved isolation of the thermometer from some common types of noise such as JN noise, current noise, and thermal noise. Using Eq. (4), the detection circuit NEP for the Meissner-TES may be written as $NEP_{Meissner}^2 = [S_V/\mathscr{R}_V^2]$, where S_V is the spectral density of the SQUID voltage noise. The responsivity is $\mathscr{R}_V \equiv (\delta V/\delta P) = (\delta V/\delta T)\cdot(\delta P/\delta T)^{-1} \equiv G^{-1}\cdot(\delta V/\delta T)$. Thus, the NEP for the Meissner-TES is $NEP_{Meissner} = (\sqrt{S_V}\cdot(\delta V/\delta T)^{-1}\cdot G)$. From Ref. 8, the measured values are $(\delta V/\delta T) = 5.91\times10^4$ V/K and $\sqrt{S_V} = 1.33\times10^{-4}\ V/\sqrt{Hz}$ near 10 Hz. Using the measured value of thermal resistance[52] from this work, $G^{-1} = 4700$ K/mW, the result is $NEP_{Meissner} = 0.48\ fW/\sqrt{Hz}$, which is a factor of 14 *smaller* than the phonon NEP in Fig. 4. Thus, the Meissner-TES detection circuit has the potential for sub-phonon NEP and therefore may enable the exploration of a new regime in cryogenic radiometry.

The experimental data in Fig. 4 were acquired in closed-loop operation, which means that the operation of the excitation circuit and the operation of the detection circuit are not entirely independent. If an improved detection system is used, such as the resistive SC-TES or Meissner-TES described above, this may also reduce the NEP for the excitation circuit through the electronic feedback. An improved detection system will reduce the lower limit of the excitation power, P_H, because at present this is determined by the precision of the detection measurement in closed-loop operation. For this work, the lower limit of the excitation power was about $P_H = 17$ pW, as shown in Fig. 4. The experimental NEP for the excitation circuit, which is expressed in Eq. (5) and displayed in Fig. 4, decreases with decreasing excitation power. Extrapolating the relation (5) to $P_H = 1$ pW assuming the other factors are unchanged, the resulting value for the NEP is approximately 14 fW/$\sqrt{\text{Hz}}$, which is about a factor of 2 larger than the fundamental phonon noise floor in Fig. 4. Therefore, assuming an improved detection system such as the Meissner-TES,[8] and perhaps improved feedback electronics, it is realistic to envision an excitation circuit NEP that is near or below the phonon noise floor, $\text{NEP}_{\text{phonon}} = 6.5$ fW/$\sqrt{\text{Hz}}$, for excitation powers in the vicinity of 1 pW.

V. CONCLUSION

A CR device, intended for use as part of an ACR, was measured at low temperature. The design of the CR device is based on the ACRII[19] previously employed at NIST. The CR device measured in this work includes reduced physical dimensions designed to be commensurate with the expected reduction in the thermal conductance of the thin-walled polyimide-tube thermal link, in order to minimize the thermal time constant.

Cryogenic measurements were performed at two discrete temperatures, $T_0 = 4.311$ K and $T_0 = 1.885$ K. The lower temperature is at or near the temperature setpoint for a radiometer of this type used as a thermal-detector-based standard for infrared radiant power. For the measurements at $T_0 = 1.885$ K presented in this work, the measured thermal resistance or thermal responsivity was $G^{-1} = 4700 \pm 200$ K/mW and the measured natural thermal time constant was $\tau = 14 \pm 2$ s.

These measured values may be compared with the values obtained at 2.2 K for the ACRII,[19] for which the measured thermal responsivity was 210 K/mW and the measured natural thermal time constant was 17 s. A more direct comparison of the values at the same temperature of 2.2 K may be estimated by assuming a temperature dependence using the data presented in this work. Interpolation of the data presented in this work yields the estimated values of $G^{-1} = 4500$ K/mW and $\tau = 20$ s. Thus, even with this approximate normalization to 2.2 K, the interpolated thermal responsivity is more than a factor of 20 larger for the ACRII, while the interpolated thermal time constant remains less than or about 20 s. Therefore, the desired objective has been achieved, as we have demonstrated a significant increase in the thermal responsivity while maintaining the thermal time constant, which may enable exploration of a new regime in cryogenic radiometry.

In order to understand the possibilities and challenges associated with the transition from the present work to the fundamental-noise-limited regime, we performed a thorough noise analysis of the excitation and detection circuits of the cryogenic radiometer device. The fundamental-noise-limited regime is the limit of an ideal[1] thermal detector, where the fundamental noise floor is due to fluctuations in the temperature of the active element, which is known as phonon noise. To realize the fundamental-noise-limited regime, the magnitudes of the technical noise sources must be reduced below the magnitude of phonon noise, which is 6.5 fW/$\sqrt{\text{Hz}}$ for the experimental parameters measured in this work.

The noise analysis yielded several important conclusions. For the cryogenic radiometer device presented in this work, the experimental NEP for the excitation circuit was about an order of magnitude larger than the fundamental phonon noise floor. The calculated JN noise limit for the excitation circuit is below the phonon noise floor over the relevant range of electrical power. Realizable modifications to the excitation circuit could therefore reduce the noise in the excitation circuit below the phonon noise floor. In contrast to the excitation circuit, the detection circuit is nearly JN-noise-limited, where the temperature sensor is a resistive thermometer. The detection circuit JN-noise limit is more than two orders of magnitude larger than the fundamental phonon noise floor. Therefore, conventional resistive thermometry is unlikely to approach the phonon noise floor, motivating consideration of alternative detectors. A possible alternative thermometer is a SC TES based on either the resistive or magnetic SC transition. It was shown that a resistive SC-TES results in significantly reduced noise compared with conventional resistive thermometry. However, reduction of the resistive SC-TES JN noise to or below the phonon noise floor appears to be challenging. Noise analysis for a SC-TES based on the magnetic transition, which we developed in our laboratory and refer to as the Meissner-TES,[8] results in a NEP that is more than an order of magnitude smaller than the phonon noise floor. The combination of reduced technical noise in the excitation circuit and implementation of the Meissner-TES in the detection circuit, may enable realization of the ultimate objective, which is the realization of a cryogenic radiometer device operating at or near the fundamental phonon noise floor.

[1] R. W. Boyd, *Radiometry and the Detection of Optical Radiation* (John Wiley and Sons, 1983).
[2] S. P. Langley, Nature (London) **25**, 14 (1881).
[3] C. Enss and D. McCammon, J. Low Temp. Phys. **151**, 5 (2008).
[4] G. C. Hilton, "Low temperature detectors: Principles and applications," AIP Conf. Proc. **1185**, 3–5 (2009).
[5] F. Simon, Nature (London) **135**, 763 (1935).
[6] M. A. Dobbs *et al.*, Rev. Sci. Instrum. **83**, 073113 (2012).
[7] M. Galeazzi, IEEE Trans. Appl. Supercond. **21**, 267 (2011).
[8] S. I. Woods, S. M. Carr, T. M. Jung, A. C. Carter, and R. U. Datla, J. Appl. Phys. **108**, 024505 (2010).
[9] D. Goldie *et al.*, J. Appl. Phys. **103**, 084509 (2008).
[10] B. Cabrera, J. Low Temp. Phys. **151**, 82 (2008).
[11] F. Giazotto *et al.*, Rev. Mod. Phys. **78**, 217 (2006).
[12] K. D. Irwin and G. C. Hilton, "Transition-edge sensors," in *Cryogenic Particle Detection*, edited by C. Enss (Springer-Verlag, 2005), Vol. 99, p. 63–149.
[13] D. McCammon, "Thermal equilibrium calorimeters - An introduction," in *Cryogenic Particle Detection*, edited by C. Enss (Springer-Verlag, 2005), Vol. 99, pp. 1–34.

[14]P. L. Richards, J. Appl. Phys. **76**, 1 (1994).
[15]K. Angstrom, Phys. Rev. **1**, 365 (1894).
[16]F. Kurlbaum, *Die Thaetigkeit der Physikalisch-Technischen Reichsanstalt in den Jahren* (Physikalisch-Technischen Reichsanstalt (PTR), Braunschweig, Federal Republic of Germany, 1891), Vol. 6.
[17]F. Hengstberger, *Absolute Radiometry* (Academic Press, Inc., San Diego, CA, 1989).
[18]R. U. Datla, K. Stock, A. C. Parr, C. C. Hoyt, P. J. Miller, and P. V. Foukal, Appl. Opt. **31**, 7219 (1992).
[19]A. C. Carter, S. R. Lorentz, T. M. Jung, and R. U. Datla, Appl. Opt. **44**, 871 (2005).
[20]J. A. Fedchak, A. C. Carter, and R. U. Datla, J. Res. Natl. Inst. Standards Technol. **111**, 325 (2006).
[21]J. M. Houston and J. P. Rice, Metrologia **43**, S31 (2006).
[22]C. D. Reintsema, J. A. Koch, and E. N. Grossman, Rev. Sci. Instrum. **69**, 152 (1998).
[23]J. P. Rice, S. R. Lorentz, R. U. Datla, L. R. Vale, D. A. Rudman, M. L. C. Sing, and D. Robbes, Metrologia **35**, 289 (1998).
[24]Z. M. Zhang, S. R. Lorentz, J. P. Rice, and R. U. Datla, Metrologia **35**, 511 (1998).
[25]Z. M. Zhang, R. U. Datla, S. R. Lorentz, and H. C. Tang, Trans. ASME - J. Heat Transfer **116**, 993 (1994).
[26]S. R. Lorentz and R. U. Datla, Metrologia **30**, 341 (1993).
[27]N. A. Tomlin, J. H. Lehman, and S. Nam, Opt. Lett. **37**, 2346 (2012).
[28]J. Y. Cheung *et al.*, Opt. Express **19**, 20347 (2011).
[29]B. Sanguinetti *et al.*, Phys. Rev. Lett. **105**, 080503 (2010).
[30]S. V. Polyakov and A. L. Migdall, J. Mod. Opt. **56**, 1045 (2009).
[31]S. I. Woods, S. M. Carr, A. C. Carter, T. M. Jung, and R. U. Datla, Proc. SPIE **7742**, 77421P (2010).
[32]A. C. Carter, R. U. Datla, S. I. Woods, and T. M. Jung, Proc. SPIE **7021**, 70210S (2008).
[33]A. C. Carter, S. I. Woods, S. M. Carr, T. M. Jung, and R. U. Datla, Metrologia **46**, S146 (2009).
[34]S. M. Carr, S. I. Woods, T. M. Jung, A. C. Carter, and R. U. Datla, Proc. SPIE **7298**, 72983Y (2009).
[35]Identification of particular manufacturers in this paper does not imply endorsement by the National Institute of Standards and Technology (NIST).
[36]LakeShore germanium resistance temperature sensor model GR-200A-2500-CD-1.4B. Technical specifications are available at http://www.lakeshore.com.
[37]The polyimide tubing used for the thermal link was manufactured by RiverTech Medical, LLC. The base material is Pyre-M.L. RC5019 Wire Enamel, which is 15%-16% Polyamic Acid of Pyromellitic Dianhydride/4,4-Oxydianiline, from Industrial Summit Technology Corporation (www.istusa.com).
[38]B. N. Taylor and C. E. Kuyatt, National Institute of Standards and Technology (NIST) Technical Note 1297 (NIST, 1994).
[39]The equivalent noise bandwidth for the excitation circuit is taken as $B_H = (2T_{int})^{-1} = 3$ Hz, where T_{int} is the integration time from the Agilent 3458A Multimeter User's Guide, 4th ed., 2000.
[40]The equivalent noise bandwidth for the ACRB is $B_G = 0.72$ Hz, as discussed in the document entitled "Analytical model of the analog filter in the 370" from LakeShore Cryotronics. An excitation frequency of 13.7 Hz is used as the reference frequency in the phase-sensitive detection of the resistance.
[41]H. B. Callen and T. A. Welton, Phys. Rev. **83**, 34 (1951).
[42]F. Reif, *Fundamentals of Statistical and Thermal Physics* (McGraw-Hill, New York, 1965).
[43]J. C. Mather, Appl. Opt. **21**, 1125 (1982).
[44]J. B. Johnson, Phys. Rev. **32**, 97 (1928).
[45]H. Nyquist, Phys. Rev. **32**, 110 (1928).
[46]The current noise measured in closed-loop operation was always greater than the current noise measured in open-loop operation. Thus, although closed-loop operation enables greater control compared to open-loop operation, it may necessarily introduce greater noise. The choice of operation mode and the compromise between control and noise will depend on the timescale of the desired measurement.
[47]J. E. Lukens, R. J. Warburton, and W. W. Webb, Phys. Rev. Lett. **25**, 1180 (1970).
[48]See, for example, commercially available options at http://www.hypres.com
[49]G. J. Kahan, R. B. DeLano, A. E. Brennemann, and R. T. C. Tsui, "Superconducting tin films of low residual resistivity," IBM J. Res. Development **4**, 173 (1960).
[50]R. S. Newbower, M. R. Beasley, and M. Tinkham, Phys. Rev. B **5**, 864 (1972).
[51]We developed a process to microfabricate tin thin-film meander-line SC-TES on a polyimide substrate using photolithography, magnetron sputtering, and argon ion milling to minimize edge effects (see Ref. 49). The use of a flexible substrate allows the device to be wrapped around the neck of the ACR receiver in Fig. 1(a).
[52]The stated experimental value of G from this work was obtained at a temperature of 1.885 K. The experimental values of $(\delta V/\delta T)$ and $\sqrt{S_V}$ from Ref. 8 were obtained at a temperature of 3.58 K. The quantity $(\delta V/\delta T)$ will increase with decreasing temperature, while the quantity $\sqrt{S_V}$ is nearly independent of temperature, resulting in a value of $NEP_{Meissner}$ at 1.885 K that is even smaller than the value calculated in the text.